Pergamon

Int. J. Heat Mass Transfer. Vol. 38, No. 5, pp. 833–842, 1995

0017-9310/95 $9.50+0.00

0017-9310(94)00202-9

Confined single- and multiple-jet impingement heat transfer—I. Turbulent submerged liquid jets

C. T. CHANG,† G. KOJASOY‡ and F. LANDIS
Department of Mechanical Engineering University of Wisconsin–Milwaukee, Milwaukee, WI 53201, U.S.A.

and

S. DOWNING
Sundstrand Corporation, 4747 Harrison Avenue, Rockford, IL 61125, U.S.A.

(*Received* 8 *November* 1993 *and in final form* 1 *July* 1994)

Abstract—An experimental study was conducted to determine the heat transfer for single and multiple confined and submerged impingement jets in single- and multi-phase flows. This type of heat transfer is of commercial interest in high performance finned coolers used in avionic equipment. Part I deals with single-phase liquid flows of Freon R-113 with Part II covering two-phase flows. Stagnation point and local average Nusselt numbers, suitable for design purposes, were determined as functions of the Reynolds number, the dimensionless spacing between the confining plates, and, for multiple jets, as a function of pitch spacing. The resulting correlation equations match the experimental data from ±10% to ±25%.

1. INTRODUCTION

The present study was motivated by the need for accurate multiple-jet impingement data in the design of small, high performance, finned heat transfer units also known as compact high intensity coolers (CHICs) that utilize impinging jets, vented through orifices in successive fins, as shown in Fig. 1. This system may be described as submerged and confined impingement; "submerged" because the jet discharges from an orifice into the same fluid, and "confined" because the spent jet fluid leaves between narrowly spaced plates. In actual CHIC units the heat from an external source is conducted to multiple fins, through which the coolant flows in a staggered hole arrangement. Fluid enters from the top and, after impinging on the bottom bar, leaves at right angles to the view shown.

There is a vast literature in the field, dealing mostly with free jets (liquid jet entering a gas-filled region, where no entrainment takes place) and with submerged turbulent jets (the jet fluid is the same as the surrounding fluid thus allowing for significant entrainment). Single or multiple jets may be either round or two-dimensional (slot) jets. Most multiple-jet experiments have the spent fluid discharged radially, thus providing cross-flows of differing magnitudes. As summarized by Downs and James [1] and by Chang [2], the Nusselt number vs Reynolds number correlations for various conditions obtained by the many authors may differ by a factor of 10. Even the stagnation point Nusselt number vs Reynolds number data for single-jet submerged air flows, obtained by 10 different authors [3–12] differ by more than 75%.

The major generally applicable results gleaned from the literature are:

(1) The stagnation point impingement heat transfer tends to be highest if the stagnation point is close to the end of the potential core of the emerging jet.

(2) The local heat transfer is highest at the stagnation point. It then drops radially outward although there may be a slight increase when the laminar flow becomes a turbulent wall jet.

(3) Irrespective of the fluid used, the stagnation

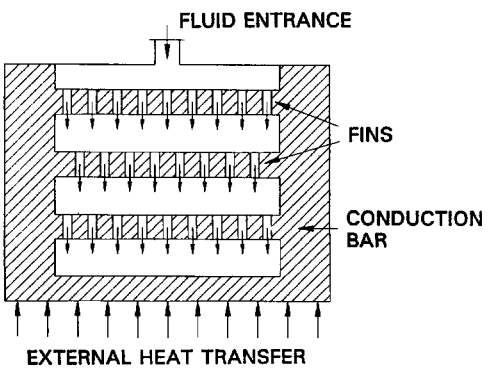

Fig. 1. Schematic cross-section through a compact high intensity cooler (CHIC) unit.

†Presently address: Yuen Ze Institute of Technology, Taiwan.

‡Author to whom correspondence should be addressed.

NOMENCLATURE

d_j	nozzle exit diameter [mm]
h	heat transfer coefficient [W m^{-2} K^{-1}]
$Nu(0)$	stagnation point Nusselt number
$\overline{Nu}(r)$	local averaged Nusselt number (averaged from $r = 0$ to r)
Pr	Prandtl number
p	pitch spacing (mm)
$\dot{q}''$	heat transfer rate per unit area [W m^{-2}]
R	radius of diffusion plate for single-jet tests
r	radial distance from stagnation point (mm)
Re_j	jet Reynolds number, based on nozzle exit diameter and velocity
T	temperature [°C]
z	plate spacing (mm) or axial direction.

Subscripts

b	refers to fluid bulk condition
e	region 0, 1 or 2 for multiple-jet thermocouple readings
o	stagnation point
w	refers to wall conditions.

Superscript

$^-$	average value.

point Nusselt number varies approximately as the Reynolds number (based on emerging jet diameter and velocity) to the 0.58 power.

(4) Free stream turbulence can increase the heat transfer significantly.

The recent numerical and experimental slot jet study of Kunugi *et al.* [13] indicates strong recirculation effects induced by close spent jet confinement. Garimella and Rice [14] performed laser sheet visualization tests on submerged and confined cylindrical jets using FC77 at jet Reynolds numbers of about 15000. They found that the entrainment vortex became pronounced at plate spacing values of $10 > z/d_j > 8$ and with actual recirculation occurring once $z/d_j < 5.0$. Thus, when compared to free jets, significant changes in heat transfer coefficients, both at and away from the stagnation point, should be expected.

The purpose of the present study was to uniquely relate multiple confined jet impingement to single-jet behavior and to lay the basis for a two-phase impingement study. Thus, it was decided to use a single working fluid (R-113) and to utilize the same experimental test setups for both the single- and the highly pressured two-phase flows. This required compromises in installation and instrumentation, both of which became more complex (and the results somewhat less accurate) than would have been the case if only single-phase tests had to be performed.

2. EXPERIMENTAL SETUP

2.1. *Overall test loop*

In the test loop, illustrated in Fig. 2, liquid Freon 113 (R-113) was pumped from a storage/degassing tank through steam and electric preheaters to a series of valves. For the tests reported here, the heaters provided a subcooled liquid at the test section. All test sections, including those for single- and multiple-jet assemblies, were fitted into a cylindrical, flanged pipe unit 11.43 cm long and 11.43 cm diameter. This unit, together with an approach straightening section, was mounted on a swing linkage. It was coupled upstream through flexible tubing to the flashing valves while downstream it was connected flexibly to an after-cooler/condenser. This arrangement permitted tests to be run with the impingement jet upward, downward and horizontal. The cooled R-113 then passed through a flow meter of appropriate size before being returned to the storage tank. The mass flow through the test section was controlled by the valves upstream of the test section and two by-pass valves. Whenever the test geometry was changed, the system was run for about 24 h to remove entrapped air through the degassing tank and bleed valves.

The absolute accuracy of the thermocouples, apart from any biasing installation errors, was estimated to be ± 0.2°C with a differential accuracy for readings in the same test of ± 0.06°C. Pressure measurements were within ± 3000 Pa. The flow meter accuracy ranged from 1 to 2%.

2.2. *Single-jet test setup*

For the single-jet experiments, the test section assembly cross section is shown in Fig. 3. The fluid entered through a nozzle in the "nozzle plate" to impinge upon the "target plate." Both plates were 76.2 mm diameter, 3 mm thick, copper disks located with a separation layer of mica over a thin cut-foil resistance heater, 66.6 mm in diameter. The heater was tightened to the copper plate by a backing plate with bolts and nuts. Good thermal contact was assured by silicon grease. The surfaces in contact with the cooling fluid were nickel plated. All heating sections were backed by Fluorosint to insulate against axial heat conduction. Different height spacers allowed for various separation distances between nozzle and target plates.

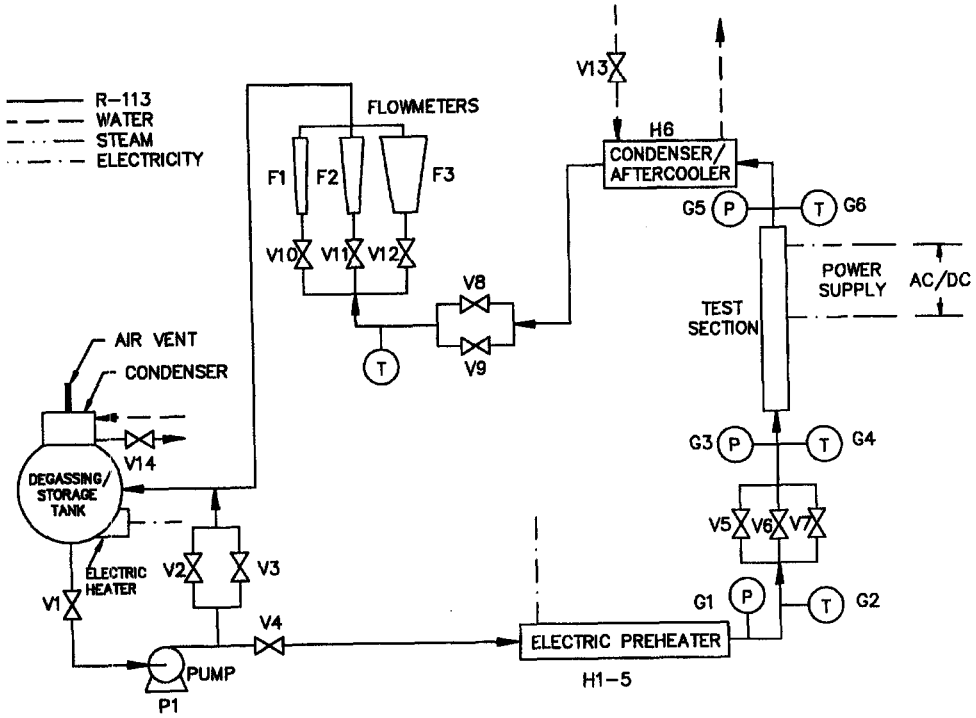

Fig. 2. Schematic diagram of test loop.

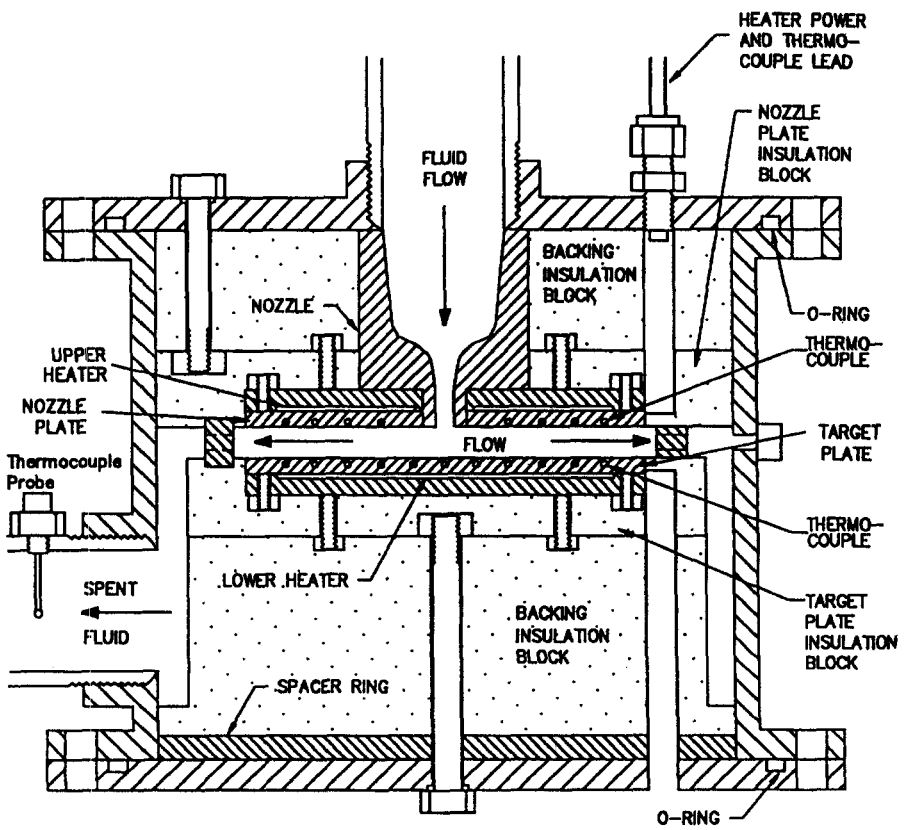

Fig. 3. Cross-section of single-jet heat transfer test section assembly.

After impingement, the fluid moved radially outward in the inter-plate space and eventually left the assembly. Upstream temperature and pressure measurements were taken directly after the straightening section. Fluid temperatures were also recorded at the test section exit and pressures were recorded at the test section sidewall between the nozzle and target plates.

Two sets of five thermocouples, set 90° apart, were embedded in the target diffusion plate at radial locations of 3.2, 8.0, 14.3, 22.2 and 30.5 mm from the center where a single stagnation point thermocouple was seated. All thermocouples were at a depth of 1 mm from the impingement surface. Since, in the actual high intensity CHIC unit, heat is also transferred from the nozzle plate, a corresponding nozzle plate heater was constructed with two sets of four thermocouples embedded again at a depth of 1 mm, but at only four radial locations (9.5, 14.3, 20.6 and 28.6 mm from the center). The AC power for the heaters was controlled by two rheostats, one for the nozzle plate and one for the target plate. The voltage drop across the heating element was measured directly while the current was noted via a calibrated shunt.

2.3. *Multiple-jet test setup*

A different design had to be employed for the multiple-jet testing. Here the heating unit consisted of a 0.0254 mm thick stainless steel strip, glued on a Fluorosint substrate. As shown in Fig. 4(a), the target plate consisted of 36 holes, laid out in a 6×6 array with 10 mm pitch spacing. The holes, drilled through the heating plate and substrate, were originally 1.0 mm diameter, subsequently drilled out to 2.0 mm. The diagram also shows the thermocouple locations. Fluid entered through the nozzle plate, which had a corresponding hole arrangement of 25 holes in a 5×5 array, off-set so that the impingement points on the target plate would be in the middle of four drain holes. Thermocouples, arranged as in the target plate, were also incorporated.

Heating was by direct current fed to the steel sheet through copper bus bars. A sectional view of the assembly is given in Fig. 4(b). All thermocouples were electrically insulated from the heating strips by a thin (about 0.02 mm thick) epoxy coat between the thermocouple beads and the heater.

Although the thermocouple arrangement, which was symmetric about the impingement point, should have led to identical dual sets of temperatures, this was not uniformly found to be the case. Slight differences in the epoxy thickness separating the bead from the heating sheet may have contributed to these measured temperature differences. After considerable testing, it was decided to use only the highest temperature read at any location, yielding the lowest heat transfer coefficient. This may have underestimated the actual heat transfer coefficient by at most 10–12%.

For both single- and multiple-jet runs, the whole test section assembly was insulated. Separate "dry" runs showed that for a given maximum diffusion plate temperature the heat loss through the insulation was always less than 3% of the total power. This heat loss was accounted for in the test energy balance.

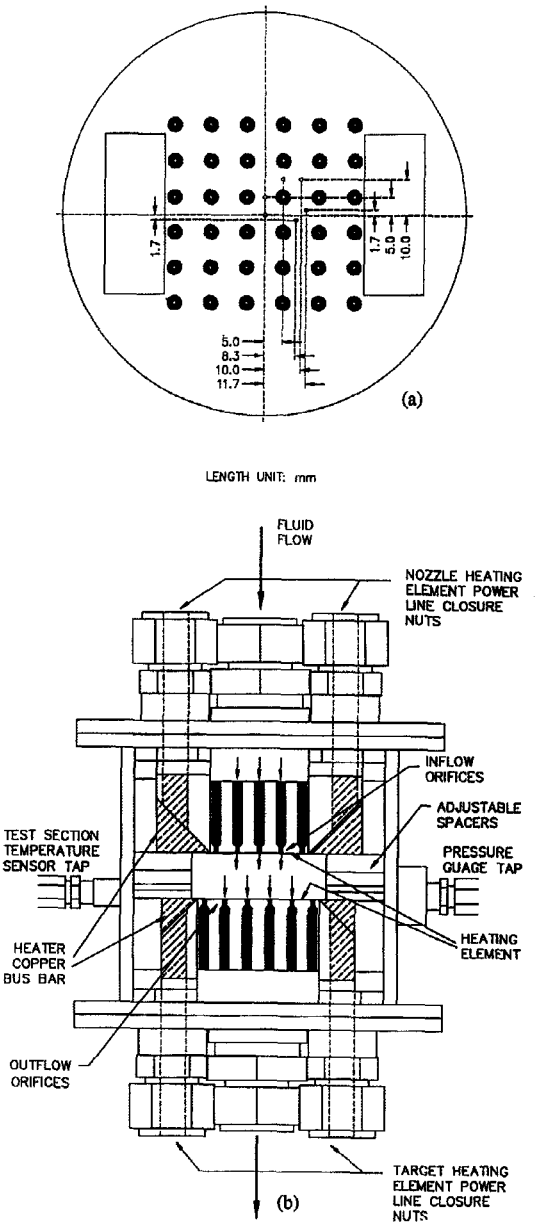

Fig. 4. Multi-jet assembly: (a) target plate hole and thermocouple layout; (b) assembly cross-section.

3. DATA REDUCTION

3.1. *Single-jet impingement data*

For the single-jet impingement data, the heat transfer to the Freon could be computed at any radial section if the local heat flux and the local plate surface temperature were known. Due to the strong heat distributing effect of the copper diffusion plate, the axial flux at the heater and plate top was assumed to be

uniform. The outer portion, where the diffusion plate was larger than the heating unit (to allow for clamping), was assumed to be insulated at the side and bottom [see Fig. 5(a)]. Although some radial and axial heat flux did actually occur, this was at radius values of beyond the range of interest for a CHIC unit.

To determine the radial temperature distribution along the diffusion target plate surface in contact with the fluid, a least square fourth-order polynomial was fitted through the six data points (stagnation point reading and average of other two thermocouple readings at the same radius). This was subject to the requirement that the radial heat flux be zero at the stagnation point and at the outer edge of the diffusion plate. A typical result for a high heat flux case is illustrated in Fig. 5(b).

Since the flow between narrow confining plates is closer to an internal passage flow rather than a boundary layer flow, a reference temperature other than the jet entry temperature should be used in defining the heat transfer coefficient. In the absence of a more suitable reference, the one-dimensional flow local bulk temperature was selected. This was computed via an energy balance by adding the temperature rise due to heating from $r = 0$ to $r = r$ to the inlet temperature. The local heat transfer coefficient could then be calculated as follows

$$h(r) \equiv \dot{q}''(r)/[T_w(r) - T_b(r)] \quad (1)$$

where $h(r)$, $\dot{q}''(r)$, $T_w(r)$ and $T_b(r)$ are the local heat transfer coefficient, local heat flux, local plate surface temperature and local bulk fluid temperature, respectively.

While local heat transfer coefficients may be of some interest, of greater utility in design (and more accurate) is the local averaged heat transfer coefficient or Nusselt number, defined as the average value between the stagnation point and the local radial distance, r. The data are presented in terms of this local averaged coefficient $\bar{h}(r)$, or as the local averaged Nusselt number, $\overline{Nu}(r)$, defined by

$$\bar{h}(r) \equiv \overline{\dot{q}''}(r)/[\overline{T_w}(r) - T_b(r)] \quad \overline{Nu}(r) \equiv \bar{h}(r)\, d_j/k \quad (2)$$

where the parameters are calculated as area averages by

$$\overline{\dot{q}''}(r) \equiv \left(\frac{2}{r^2}\right)\int_0^r \dot{q}''(r)\, r\, dr; \quad \bar{T}(r) \equiv \left(\frac{2}{r^2}\right)\int_0^r T(r)\, r\, dr. \quad (3)$$

The actual calculations of the local and local averaged heat transfer coefficient for a system as illustrated in Fig. 5(a) involved the use of the fourth-order polynomial along the target plate and J-type Bessel functions. An error arises by assuming that the thermocouple data for the least square fit are taken at the surface rather than 1 mm below it. A separate analysis concluded that, over the full range of test conditions, this could lead to an underestimate of between 0.65 and 2.6% in the local heat transfer coefficients.

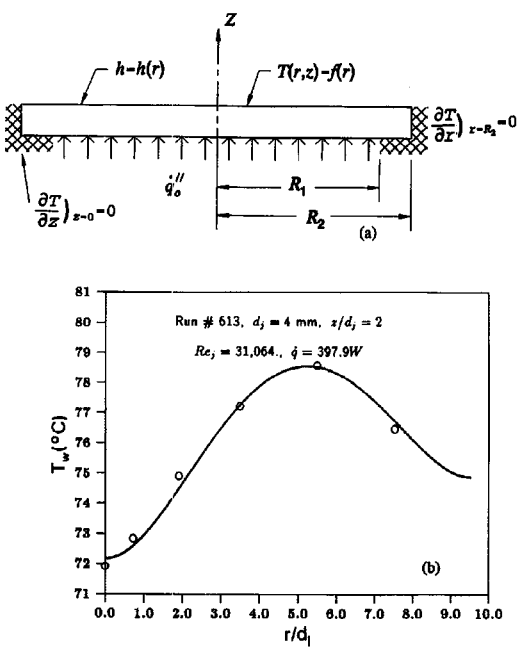

Fig. 5. Temperature distribution in single-jet target plate: (a) assumed heat conduction boundary conditions used for analysis; (b) typical fourth-order target plate temperature fit with high heat flux.

3.2. *Multiple-jet data*

In the multi-jet case, only a small number of thermocouples (three in any radial direction) could be accommodated in any square impingement cell. For comparison with single-jet data, each 10 mm × 10 mm cell was matched by an equal area circle of 11.3 mm diameter. The three thermocouple readings were then assumed to reflect the center temperature of rings of influence (0.63 mm^2 for the stagnation region, 59.1 mm^2 for the next ring and 40.2 mm^2 for the outer ring).

4. RESULTS AND DISCUSSION

4.1. *Single-jet heat transfer*

Figure 6(a) shows typical values of single-phase local averaged Nusselt numbers, $\overline{Nu}(r)$, computed from the temperature curve fits, as a function of r/d_j for several values of jet Reynolds number at a given value of z/d_j. The computed points were chosen so that their locations were close to the actual thermocouple locations. Correlations for $\overline{Nu}(r)$, developed subsequently, are included as solid lines. The behavior illustrated is typical of all jet diameters and z/d_j ratios tested. $\overline{Nu}(r)$ is highest at the stagnation point, where local and local averaged Nusselt numbers agree, and then drops off in the wall jet region with increasing

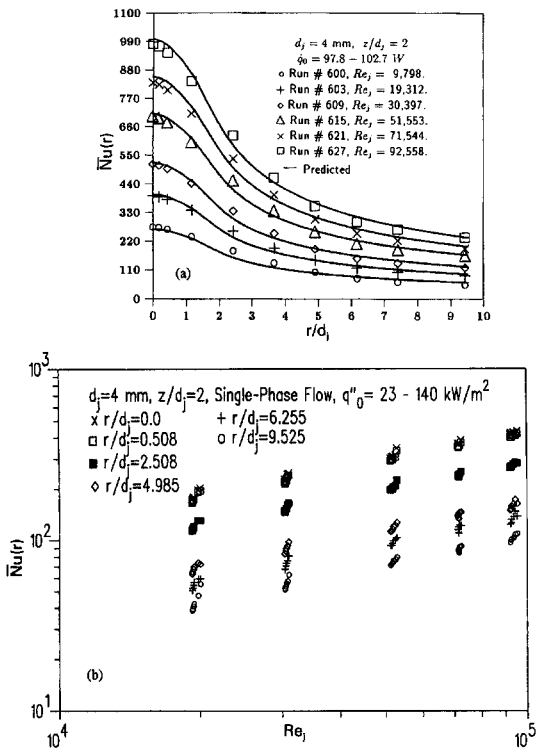

Fig. 6. Local average Nusselt number $\overline{Nu}(r)$ for single-jet heat transfer at $z/d_j = 2.0$. (a) Computed local averaged Nusselt number vs distance from stagnation point r/d_j (solid lines are results of equations (9) and (10)). (b) Effect of jet Reynolds number Re_j on local average Nusselt number.

radius. $\overline{Nu}(r)$ and the heat transfer coefficients increase with increasing Re_j.

To arrive at appropriate correlations, log $\overline{Nu}(r)$ was first plotted against the log of the jet Reynolds number (Re_j) for various values of r/d_j and for various power settings at a fixed plate spacing; for $z/d_j = 2$ illustrated in Fig. 6(b). Corresponding graphs were developed for other values of z/d_j. These graphs, all of which cover turbulent flow, clearly showed that a single power law relation between local averaged Nusselt number $\overline{Nu}(r)$ and jet Reynolds number held for all test conditions. Since over the test range the Prandtl number for R-113 was essentially constant, a separate Prandtl number dependency could not be determined. Thus, while in general there are functional relationships of the form

$$Nu(0) = f(Re_j, Pr, z/d_j)$$

and

$$\overline{Nu}(r) = f(Re_j, Pr, z/d_j, r/d_j) \quad (4)$$

the tests suggested that the ratio $\overline{Nu}(r)/Nu(0)$ was only a function of the geometry, i.e.

$$\overline{Nu}(r)/Nu(0) = f(z/d_j, r/d_j). \quad (5)$$

As expected, the experiments also confirmed that, for single-phase flows, the Nusselt number remained essentially independent of heat flux.

The Prandtl number dependence for liquid jet impingement has been characterized with exponents ranging from 0.33 to 0.487 by Jiji and Dagan [15], Ma and Bergles [16] and Metzger *et al.* [17]. A value of 0.4 was chosen as representative for this study.

A plot of the stagnation point Nusselt number, $Nu(0)$, divided by $Pr^{0.4}$ against jet Reynolds number for the test conditions $1.5 \leqslant z/d_j \leqslant 4.0$ is shown in Fig. 7. As evidenced by the figure, the effect of the z/d_j on Nusselt number shows only a small decrease in $\overline{Nu}(r)$ with increasing nozzle-to-plate spacing. This does not match the free jet data of many investigators who observed a peak in $Nu(0)$ vs z/d_j within the potential core ($z/d_j \approx 5$–7), although even for free jets there is no full agreement. For a submerged liquid jet, Ma and Bergles [15] reported no z/d_j dependence, neither did Serizawa *et al.* [18] for confined impingement flow. Thus the small dependence of $Nu(0)$ on z/d_j observed in the present study of confined flow (with its high recirculation) appears appropriate although additional clarifying work would be useful.

The small z/d_j variation shown in Fig. 7 was utilized in the correlation of the stagnation point Nusselt number given by

$$Nu(0) = 0.660 Re_j^{0.574} Pr^{0.4} (z/d_j)^{-0.106}. \quad (6)$$

The comparison of experimental stagnation point Nusselt numbers with the results predicted by equation (6) is shown in Fig. 8 together with $\pm 10\%$ confidence limits. Eliminating the z/d_j effect over the actual test range $1.5 \leqslant z/d_j \leqslant 4$ would not lead to a significant error.

In order to find the specific correlation suggested by equation (5), log $[\overline{Nu}(r)/Nu(0)]$ was plotted on Fig. 9 vs log r/d_j for all values of z/d_j. The data scatter is indicated by the band height. No consistent variation with z/d_j could be detected; the region of largest data scatter occurred far from the stagnation point where z/d_j effects should be minimal. Thus, the final cor-

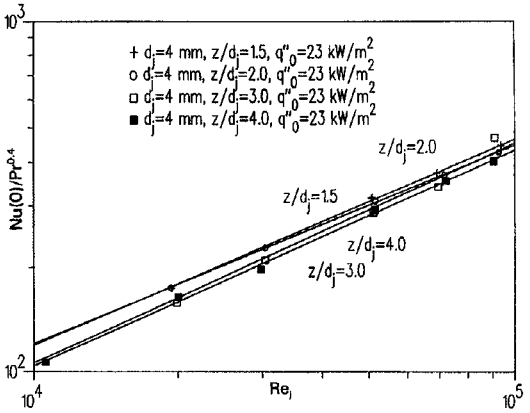

Fig. 7. Modified stagnation point Nusselt number vs jet Reynolds number at various values of z/d_j for single-jet heat transfer.

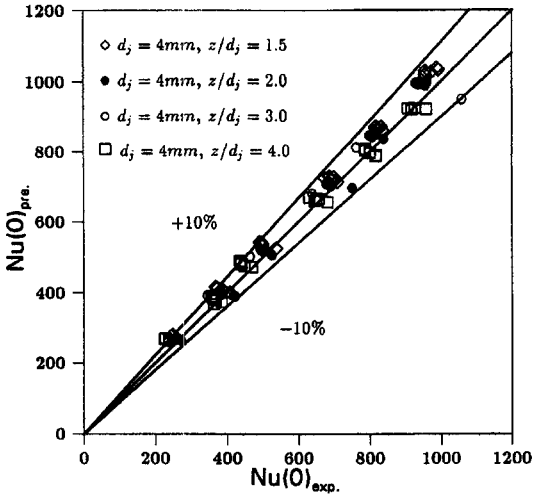

Fig. 8. Correlation results of stagnation point Nusselt number (from equation (6)) vs experimental Nusselt numbers for single-jet data.

relation of $\overline{Nu}(r)/Nu(0)$ was found to be a function of r/d_j only. However, the figure suggests a discontinuity in the r/d_j effect with a large negative power applicable once r/d_j exceeds 1.25. This change may be due to the development of the turbulent wall jet, augmented by the strong recirculation vortex in a narrowly confined jet.

A detailed examination of all data yielded

$$\overline{Nu}(r)/Nu(0) = [1+0.1147(r/d_j)^{1.81}]^{-1} \quad \text{when } r/d_j \leqslant 1.25 \qquad (7)$$

$$\overline{Nu}(r)/Nu(0) = 1.0632(r/d_j)^{-0.62}; \quad r/d_j > 1.25. \qquad (8)$$

These correlations were then again compared to all the original computed data as shown in Fig. 10(a) for small values of r/d_j and in Fig. 10(b) for larger r/d_j. Close to the stagnation point the correlations fit all data to within $\pm 10\%$; at larger radial distances the agreement is within $\pm 25\%$.

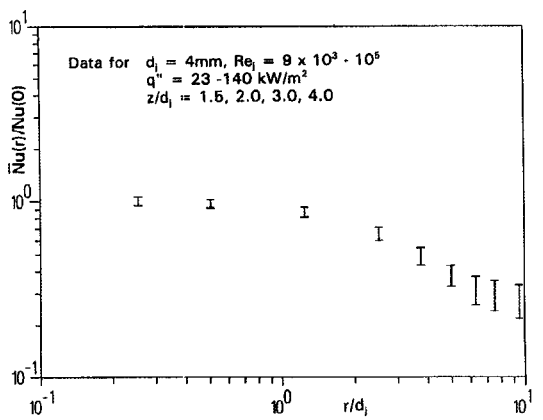

Fig. 9. Experimental local average Nusselt number divided by stagnation point Nusselt number vs radial distance, r/d_j, for single-jet heat transfer at various values of z/d_j. All data fall within the vertical ranges shown.

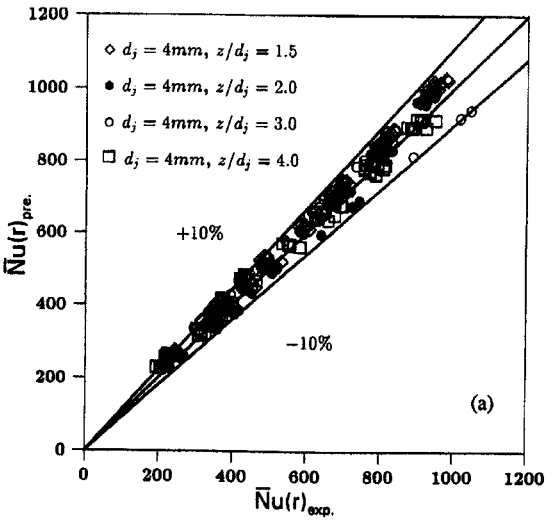

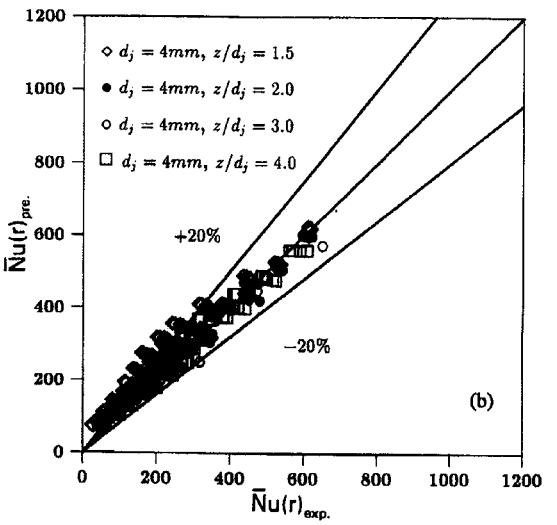

Fig. 10. Comparison of correlation of local average Nusselt number with experimental Nusselt number in single-jet heat transfer: (a) for $r/d_j \leqslant 1.25$; (b) for $r/d_j > 1.25$.

Combination of equations (7) and (8) with equation (6) leads to the overall correlations for the single submerged jet given by

$$\overline{Nu}(r) = 0.660 Re_j^{0.574}\, Pr^{0.4}\, (z/d_j)^{-0.106} \times [1+0.1147(r/d_j)^{1.81}]^{-1} \qquad (9)$$

for $r/d_j \leqslant 1.25$, while for larger values of r/d_j

$$\overline{Nu}(r) = 0.7017 Re_j^{0.574}\, Pr^{0.4}\, (z/d_j)^{-0.106}\, (r/d_j)^{-0.62} \qquad (10)$$

holds. These correlations are plotted as solid lines in Fig. 6(a) for $z/d_j = 2$. All correlations are based on using R-113 over the range: $9500 \leqslant Re_j \leqslant 110\,000$, $1.5 \leqslant z/d_j \leqslant 4.0$ and $6.0 \leqslant Pr \leqslant 8.5$. An uncertainty analysis for the experimental Nusselt numbers suggested that these are accurate to within $\pm 20\%$ for single-jet flow over most of the test range. As expected

for single-phase jet impingement, flow orientation (up, down or horizontal) did not influence the results.

4.2. *Multiple-jet heat transfer*

An energy balance provided the local bulk temperature at the temperature measurement points corresponding to the middle and outer ring positions discussed previously. The stagnation point heat transfer was given by

$$h_0 = \dot{q}''/(T_{wo} - T_{inlet}) \tag{11}$$

while the local average heat transfer coefficient became

$$\bar{h}_e(r) = \overline{\dot{q}''}/[\overline{T_{we}}(r) - T_{be}(r)] \tag{12}$$

where $e = 1$ or 2 depending on the middle or outer ring selected. The mass flow rate for each jet was taken to be 1/25 of the total flow rate.

Typical data-correlated results, comparing the multi-jet stagnation point heat transfer to that of the single-jet, are shown in Fig. 11(a): corresponding results for the local average Nusselt number are given in Fig. 11(b). It is noted that single-jet data resulted in higher stagnation point heat transfer than multiple jets, while the opposite held for single-jet local average heat transfer coefficients. It is difficult to assess whether these differences are due only to changes in flow conditions or whether different experimental setups also contribute to the deviations. The increased turbulence due to the interaction of neighboring impinging jets in the multi-jet flows likely reduces the strength (and length) of the jet potential core and the stagnation point heat transfer. Increased turbulence may result in higher heat transfer along the wall jet, resulting in lower values of $Nu(0)$ with increasing z/d_j as appears to be borne out by the test results. For a given value of Re_j, smaller values of z/d_j should increase the radial flow velocity in a confined flow between two plates and presumably increase the heat transfer. To determine this effect, the ratio $\overline{Nu}(r)_{multi\text{-}jet}/\overline{Nu}(r)_{single\text{-}jet}$ was plotted against z/d_j as shown in Fig. 12. Although the data are too limited for sweeping conclusions, the overall results can be effectively correlated by

$$\overline{Nu}(r)_{multi\text{-}jet} = 1.667(z/d_j)^{-0.116}\,\overline{Nu}(r)_{single\text{-}jet} \tag{13}$$

where $\overline{Nu}(r)_{single\text{-}jet}$ is obtained from either equation (9) or (10).

No significant separate influence of the pitch-to-jet diameter ratio (p/d_j) was observed for the two values of $p/d_j = 5$ and 10 tested. However, this does not imply that the multiple-jet average Nusselt number, $\overline{Nu}(r)_{multi\text{-}jet}$ is not affected by p/d_j. Using the equivalent circle data analysis, the maximum radius when used in equation (12) is directly related to the pitch, p, by

$$r = (d_j/2)[(1/\pi)\,(p/d_j)^2 - 1]. \tag{14}$$

No attempt was made to find a correlation at the stagnation point which presumably is of little interest in a multi-jet assembly. The comparison between all experimental data and the data-correlation local Nus-

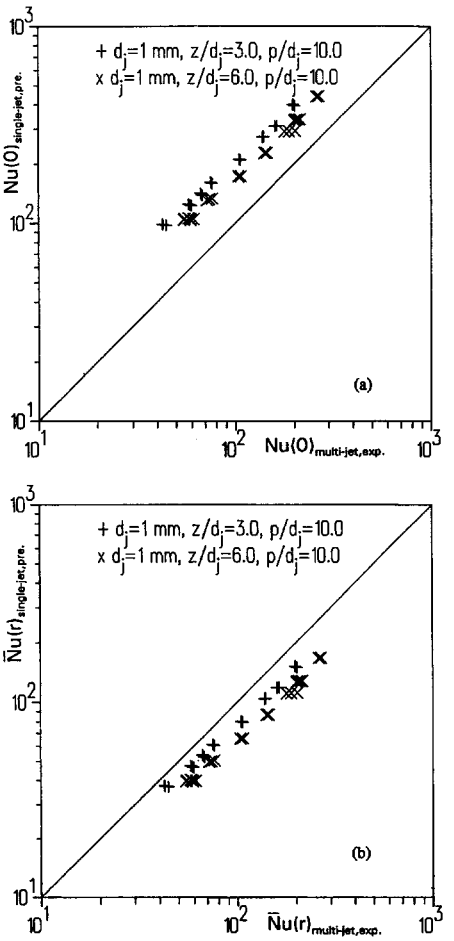

Fig. 11. Comparison between data-correlated single-jet Nusselt number vs experimental multi-jet Nusselt numbers: (a) stagnation point comparison; (b) local average Nusselt number comparison.

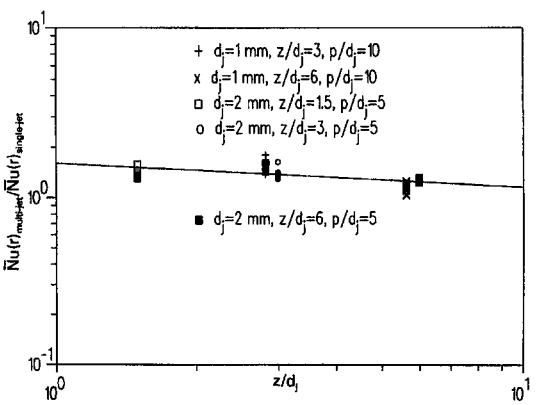

Fig. 12. Ratio of local average Nusselt number of multiple jets to local average Nusselt number for single jets.

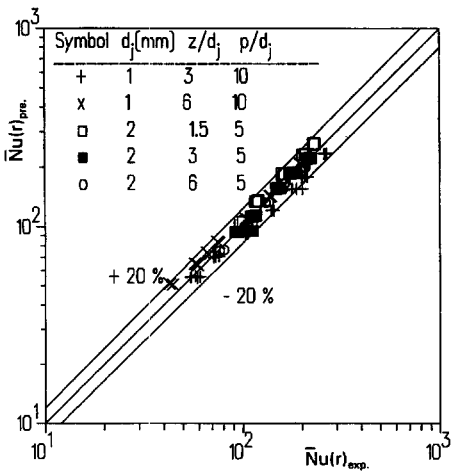

Fig. 13. Correlation comparison of multiple-jet local average Nusselt numbers vs experimental values.

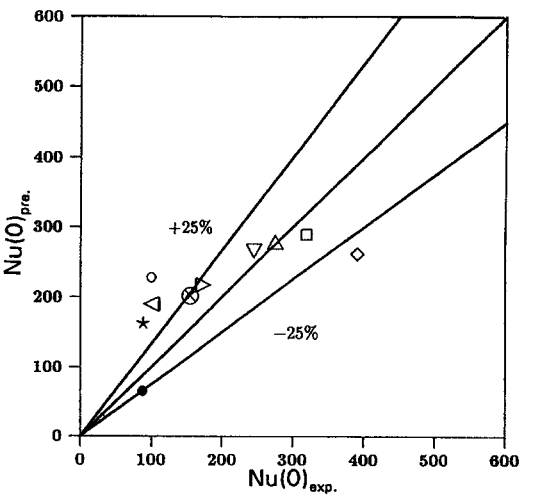

Symbol	d_j (mm)	z/d_j	Re_j	Author
○	4.6	4.0	4.0×10^4	Amano and Jensen 1982
●	6.35	7.0	5.0×10^3	Sparrow and Lovell 1980
◇	6.35	6.5	5.5×10^4	Hrycak 1982
□	22.0	4.0	6.0×10^4	Ward and Mahmood 1982
△	9.0	4.0	5.6×10^4	Gardon and Cobonque 1961
▽	9.52	4.0	5.4×10^4	Hrycak 1983
◁	19.05	4.0	2.95×10^4	Obot, Majumdar and Douglas 1979
▷	10.0	6.0	4.0×10^4	Goldstein and Timmers 1982
⊗	12.7	6.0	3.52×10^4	Goldstein and Behbahani 1982
★	6.35	2.0	2.0×10^4	Gardon and Akfirat 1965

Fig. 14. Single-jet stagnation point Nusselt number results of other authors compared with present correlation results.

selt numbers is shown in Fig. 13. All test results are expected to be accurate to within $\pm 25\%$ and fall within $\pm 20\%$ of the correlation. Again, as expected, no influence of flow direction could be detected.

5. COMPARISON WITH THE WORK OF OTHERS

As has already been suggested, the behavior of confined jets may differ sufficiently from the most often reported free jet (liquid into air) or submerged jet (air into air or water into water) data to make the value of direct comparisons questionable. The results of [13] dealing with confined submerged single air jets were presented after this study was completed. These low Reynolds number (maximum $Re_j = 8000$) experiments, used primarily to confirm numerical solutions, do not cover the higher Reynolds number range and the higher Prandtl numbers of the present work and the results are not presented in terms of correlations. Reference [14] is more comparable to the present tests and clearly shows the importance of the recirculation vortex.

Yet, it may be of practical value to try and predict the experimental results of others with the correlations. It is assumed that the Prandtl number effect can be covered by using Nusselt number divided by $Pr^{0.4}$. The air-in-air unconfined stagnation point Nusselt number results selected from ten previous investigations and covering approximately the same range of Re_j and z/d_j are compared to the results of equation (6) in Fig. 14. The results are at first discouraging, although they confirm the major differences in results between other investigators. While the correlation of equation (6) differs widely from the result of others in terms of the z/d_j effects, the jet Reynolds number exponent, m, is nearly constant. A value of $m \approx 0.58$ best correlated all the data examined. This agrees with the present result where m in equation (6) is 0.574. Thus most of the differences may be associated with jet confinement and the effect of the recirculation vortex.

In the multi-jet experiments reported by others, the fluid was drained from one or two sides. Here the cross-flow effect of the spent fluid significantly alters the average heat transfer coefficient. Only Hollworth and Dagan [19] and Hollworth *et al.* [20] considered arrays of impinging jets with spent fluid removal through vent holes in the target surface. However, their setups are so different from the present configuration that a direct comparison of results does not seem appropriate.

6. SUMMARY AND CONCLUSIONS

An extensive experimental study was undertaken to evaluate heat transfer characteristics for single-jet and multi-jet impingement in submerged confined liquid flows as utilized in avionic heat transfer enhancement units. The experiments covered a large range of turbulent jet Reynolds numbers with different plate spacing-to-jet diameter and orifice pitch-to-jet diameter ratios.

Single-jet data were obtained for both stagnation point Nusselt numbers and local-average Nusselt numbers to permit prediction of the average heat transfer over a region extending outward from the stagnation point. It was observed that the stagnation point Nusselt number decreases slightly with an increasing plate spacing-to-jet diameter ratio, even at ratios which would still be within the potential core in unconfined flows, thus contradicting the results of others. In the absence of further work, it is assumed

that this difference is caused primarily by the recirculation vortex in a confined flow which contributes to the breakup of the emerging jet. Multi-jet experiments clearly showed the strong jet interaction between adjacent jets. These reduced the stagnation point heat transfer compared to a single jet, but slightly increased the heat transfer away from the stagnation point. Design correlations applicable to actual multi-jet impingement units were developed.

All tests reported were conducted with highly turbulent jets; no information has been obtained for low jet Reynolds numbers which might be encountered in some CHIC designs. Although the nature of the jet interactions suggest that turbulent analyses may be applicable to Reynolds numbers lower than the conventional pipe flow transition value of 2100, extrapolation of the results to much lower values can not be recommended without further tests.

Acknowledgements—This work is based, in part, on the doctoral thesis of C. T. Chang. Support by the Advanced Technology Group of the Sundstrand Corporation is gratefully acknowledged.

REFERENCES

1. S. J. Downs and E. H. James, Jet impingement heat transfer—a literature survey, ASME Paper 87-HT-35 (1987).
2. C. T. Chang, Hydrodynamic and thermal field characteristics for two-phase jet impingement flows, Ph.D. Thesis, University of Wisconsin–Milwaukee (1992).
3. R. Gardon and J. Cobonpue, Heat transfer between a flat plate and jets of air impinging on it, *Int. Dev. Heat Transfer (ASME)*, pp. 454–460 (1961).
4. R. Gardon and J. C. Akfirat, The role of turbulence in determining the heat transfer characteristics of impinging jets, *Int. J. Heat Mass Transfer* **8**(10), 1261–1272 (1965).
5. N. T. Obot, A. S. Majumdar and W. J. M. Douglas, The effect of nozzle geometry on impingement heat transfer under a round turbulent jet, ASME Paper 79-WA/HT-53 (1979).
6. R. S. Amano and M. K. Jensen, A numerical and experimental investigation of turbulent heat transport of an axisymmetric jet impinging on a flat plate, ASME Paper 82-WA/HT-55 (1982).
7. R. J. Goldstein and A. I. Behbahani, Impingement of a circular jet with and without cross flow, *Int. J. Heat Mass Transfer* **25**(9), 1377–1382 (1982).
8. R. J. Goldstein, and J. F. Timmers, Visualization of heat transfer from arrays of impinging jets, *Int. J. Heat Mass Transfer* **25**(12), 1857–1868 (1982).
9. J. Ward and M. Mahmood, Heat transfer from a turbulent, swirling, impinging jet, *Proceedings of the Seventh International Heat Transfer Conference*, Munich, Vol. 3, pp. 401–407 (1982).
10. P. Hryczak, Heat transfer and flow characteristics of jets impinging on a concave hemispherical plate, *Proceedings of the Seventh International Heat Transfer Conference*, Munich, Vol. 3, pp. 357–362 (1982).
11. P. Hryczak, Heat transfer from round impinging jets to a flat plate, *Int. J. Heat Mass Transfer* **26**(12), 1857–1965 (1983).
12. E. M. Sparrow and B. J. Lovell, Heat transfer characteristics of an obliquely impinging circular jet, *ASME J. Heat Transfer* **102,** 202–209 (1980).
13. T. Kunugi, T. Yokomine and K. Ichimiya, Numerical and experimental study on heat transfer of an impinging turbulent plane jet with confined wall, *Heat Transfer in Turbulent Flows*— 1993, ASME HTD **246,** 25–31 (1993).
14. S. Garimella and R. A. Rice, Personal communication. To be presented as "Heat transfer in submerged and confined jet impingement," 1994 ASME Winter Annual Meeting.
15. L. M. Jiji and Z. Dagan, Experimental investigation of single-phase multi-jet impingement cooling of an array of microelectronic heat transfer, *Proceedings of International Symposium on Cooling Technology for Electronic Equipment*, Pacific Institute of Thermal Engineering, Hawaii, pp. 265–283 (1987).
16. C. F. Ma and A. E. Bergles, Boiling jet impingement cooling of simulated microelectronic chips. In *Heat Transfer in Electronic Cooling Equipment* (Edited by S. Oktay and A. Bar-Cohen), pp. 292–299. ASME, New York (1983).
17. D. E. Metzger, K. N. Cummings and W. A. Ruby, Effects of Prandtl number on heat transfer characteristics of impinging liquid jets, *Proceedings Fifth International Heat Transfer Conference*, Vol. II, pp. 20–24 (1974).
18. A. Serizawa, O. Takahashi, K. Zensaku, T. Komeyama and I. Michiyoshi, Heat transfer augmentation by two-phase bubbly flow impinging jet with a confining wall, *Proceedings Ninth International Heat Transfer Conference*, Vol. 4, pp. 93–98 (1990).
19. B. R. Hollworth and L. Dagan, Arrays of impinging jets with spent fluid removal through vent holes on the target surface—Part 1. Average heat transfer, *Trans. ASME, J. Engng Power* **102,** 994–999 (1980).
20. B. R. Hollworth, G. Lehman and Rosiczkowski, Arrays of impinging jets with spent fluid removal through vent holes on the target surface—Part 2. Local heat transfer, ASME Paper 81-HT-76.